J Digit Imaging (2015) 28:116–122
DOI 10.1007/s10278-014-9711-2

Eigenspace Template Matching for Detection of Lacunar Infarcts on MR Images

Yoshikazu Uchiyama · Akiko Abe · Chisako Muramatsu · Takeshi Hara · Junji Shiraishi · Hiroshi Fujita

Published online: 19 June 2014

Abstract Detection of lacunar infarcts is important because their presence indicates an increased risk of severe cerebral infarction. However, accurate identification is often hindered by the difficulty in distinguishing between lacunar infarcts and enlarged Virchow-Robin spaces. Therefore, we developed a computer-aided detection (CAD) scheme for the detection of lacunar infarcts. Although our previous CAD method indicated a sensitivity of 96.8 % with 0.71 false positives (FPs) per slice, further reduction of FPs remained an issue for the clinical application. Thus, the purpose of this study is to improve our CAD scheme by using template matching in the eigenspace. Conventional template matching is useful for the reduction of FPs, but it has the following two pitfalls: (1) It needs to maintain a large number of templates to improve the detection performance, and (2) calculation of the cross-correlation coefficient with these templates is time consuming. To solve these problems, we used template matching in the lower dimension space made by a principal component analysis. Our database comprised 1,143 T_1- and T_2-weighted images obtained from 132 patients. The proposed method was evaluated by using twofold cross-validation. By using this method, 34.1 % of FPs was eliminated compared with our previous method. The final performance indicated that the sensitivity of the detection of lacunar infarcts was 96.8 % with 0.47 FPs per slice. Therefore, the modified CAD scheme could improve FP rate without a significant reduction in the true positive rate.

Keywords Lacunar infarcts · Computer-aided diagnosis · Template matching · Eigenspace

Y. Uchiyama (✉) · J. Shiraishi
Department of Medical Physics, Faculty of Life Science, Kumamoto University, 4-24-1 Kuhonji, Kumamoto, Kumamoto 862-0976, Japan
e-mail: y_uchi@kumamoto-u.ac.jp

A. Abe · C. Muramatsu · T. Hara · H. Fujita
Department of Intelligent Image Information, Graduate School of Medicine, Gifu University, 1-1, Yanagido, Gifu, Gifu 501-1194, Japan

Introduction

Lacunar infarct is a type of stroke, which is caused by occlusion of deep penetrating arteries and is detected in 20 % of healthy elderly people [1]. The presence of lacunar infarcts increased risk of severe stroke [1–5]. Rotterdam Scan Study indicated adjusted hazard ratio was 3.9 [4]. In another cohort study, adjusted odds ratio was 3.66 [5]. Rotterdam Scan Study also indicated that the presence of silent brain infarcts at baseline more than doubled the risk of dementia (hazard ratio was 2.26) [6].

Cerebrovascular diseases are the third leading cause of death in Japan. A screening system for the early detection of asymptomatic brain diseases is widely used. Because of the recent progress of magnetic resonance (MR) imaging, various types of asymptomatic cerebral diseases are detected. In the screening system, the detection of asymptomatic lacunar infarcts is important because their presence indicates an increased risk of severe stroke and dementia. However, accurate identification of lacunar infarcts on MR images is often difficult for radiologists because of difficulty in distinguishing lacunar infarcts from other lesions such as enlarged Virchow-Robin spaces. Therefore, we developed a computer-aided detection (CAD) scheme for the detection of lacunar infarcts on T_1- and T_2-weighted images. Our previous CAD scheme indicated a sensitivity of 96.8 % with 0.71 false positives (FPs) per slice [7, 8]. An observer study was also conducted to evaluate the performance of radiologists without and with use of our previous CAD scheme [9]. The average

area under the receiver operating characteristic curve (AUC) values for nine radiologists improved from 0.891 (without the computer output) to 0.937 (with the computer output), and this difference was statistically significant (p=0.032). Therefore, we believe that the CAD scheme could improve the accuracy of radiologists' performance in the detection of lacunar infarcts. In the observer study, we realized the following two points: (1) Radiologists had difficulty distinguishing between lacunar infarcts and some of the FPs detected by the computer. These FPs were the main source of the detrimental effects of the CAD scheme. (2) The clear FPs had an impact on the reliability of the result of the computer. Therefore, as the next step of this study, it is important to develop a technique for eliminating such FPs.

Template matching techniques were used to distinguish between abnormal lesions and FPs [10–14]. For example, such techniques were employed for the detection of nodules in chest computed tomographic (CT) scans [10], the detection of masses in mammograms [12], the detection of colon in abdominal CT scans [14], and the identification of the same patient [15]. Although conventional template matching is useful, it has two pitfalls: (1) It needs to maintain a large number of templates to improve the detection performance, and (2) calculation of the cross-correlation (CC) coefficient with those templates is time-consuming. For example, Tourassi et al. used 1,465 templates for the detection of breast masses [13]. Li et al. used 3,313 templates for the detection of lung nodules in chest radiograms [11]. One approach to solve these problems is the eigenspace method [16], in which templates can be compressed in the lower dimension space made by a principal component analysis [17]. In addition, the computational complexity of the CC coefficients could be decreased. Moreover, if some useful information for the distinction between lacunar infarcts and FPs is extracted by the principal component analysis, the detection performance of our CAD scheme could possibly be improved as well. Therefore, in this study, we developed a method using eigenspace template matching to solve the problems described above. We also investigated whether the modified CAD scheme can improve FP rate without a significant reduction in the true positive rate.

Materials and Methods

Clinical Cases

Our database consisted of 1,143 T_1- and T_2-weighted MR images, which were selected from 132 patients (mean age, 63.4 years; age range, 28–83 years). A radiological technologist selected these image from PACS data with the criteria of suspicious abnormal cases including lacunar infarct. A head MR study includes 18 slice images. From 7 to 10 slices were manually selected based on the range of presence of lacunar infarcts, and were used in this study. The images were acquired using a 1.5-T magnetic imaging scanner (Signa Excite Twin Speed 1.5 T; GE Medical Systems, Milwaukee, WI, USA) at the Gifu University Hospital (Gifu, Japan). The T_1- and T_2-weighted images were obtained using the fast-spin-echo method with effective echo times of 8–12 and 96–105 ms, respectively, and repetition times of 300–500 and 3,000–3,500 ms, respectively. All MRIs were obtained in the axial plane with a section thickness of 5 mm with a 2-mm intersection gap, which covered the entire brain. The matrix size of the MRIs was 512×512, with a spatial resolution of 0.47 mm/pixel. The location of the lacunar infarcts were determined by an observer study with two experienced neuroradiologists [8]. Observer A selected 120 candidates for lacunar infracts, whereas the observer B selected 154 candidates. A candidates that were identified by both the neuroradiologists were considered as a "lacunar infarct." The sensitivity for the detection of lacunar infarcts was calculated based on the locations of the lacunar infarcts. On the other hand, the number of FPs per slice image was calculated based on the "non-lacunar slices." A slice was determined as non-lacunar when a point on the slice was not identified as a lacunar infarct by either of the two neuroradiologists. Our database included 93 lacunar infarcts and 1,063 non-lacunar slices.

Overall Scheme for Detection of Lacunar Infarcts

Figure 1 summarizes the automated detection method for lacunar infarcts. The unshaded parts indicate our previous techniques [8], and the shaded part indicates the proposed method. First, we segmented the cerebral parenchymal region on the basis of the region-growing technique in order to avoid false findings located outside the cerebral parenchymal region. To identify the initial candidates for lacunar infarcts, we applied top-hat transformation and multiple-phase binarization techniques to the T_2-weighted image within the segmented cerebral region. To eliminate FPs, we determined 12 features (i.e., x and y locations, signal-intensity differences in the T_1- and T_2-weighted images, nodular components from a scale of 1 to 4, and nodular and linear components from a scale of 1 to 4). Finally, rule-based schemes and a support vector machine with the 12 features were used to distinguish between lacunar infarcts and FPs. By using our previous method described above, the sensitivity of 96.8 % (90/93) with 0.76 (813/1,063) FPs per slice was obtained [8]. Before this study, we decreased the number of FPs from 0.76 to 0.71 (753/1,063) by fine-tuning the parameters of the support vector machine. By applying the proposed method to this result, we investigated the usefulness of template matching in the eigenspace.

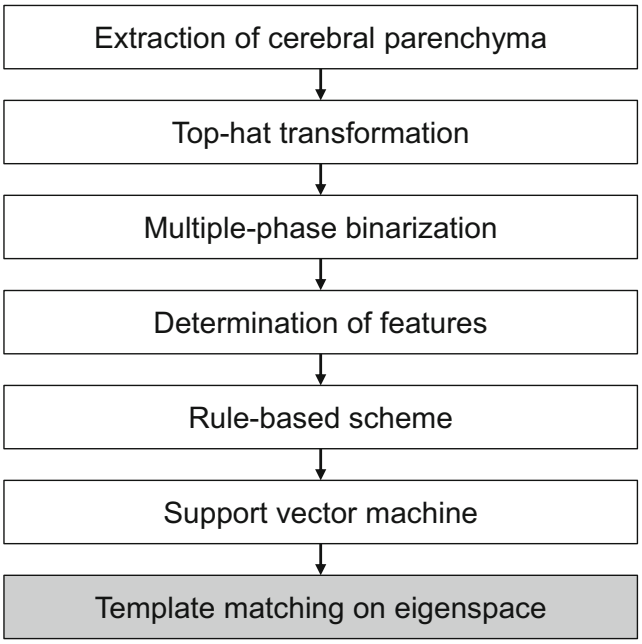

Fig. 1 Overall scheme for the detection of lacunar infarcts

Eigenspace Template Matching

From each of the candidate regions detected by our previous method, we calculated the center of gravity. The region of interest (ROI) of 51×51 around the center of gravity was subsequently selected. The numbers of lacunar infarct ROIs and FP ROIs were 90 and 753, respectively. To evaluate the proposed method, we employed twofold cross-validation [18] using these ROIs. We randomly divided the lacunar ROIs and the FP ROIs into two data sets: A and B. Set A consisted of 46 lacunar ROIs and 360 FP ROIs. Set B consisted of 45 lacunar ROIs and 393 FP ROIs. Set A was first used for training, and set B was used for testing. This was then reversed (i.e., set B was used for training, and set A was used for testing). The training means the ROIs are used as templates.

Figure 2 shows a brief overview of template matching in the eigenspace. The first step in template matching in the eigenspace is to make an eigenspace by using principal component analysis of the training data set. A 51×51-pixel ROI image in the training data set is converted into a one-dimensional array of data of 1×2,601. All converted training data arranged vertically were used as the input data of the principal component analysis. In other words, the input data become a two-dimensional array of the number of training data×2,601 variables. After the pixel values were normalized by the mean and standard deviation of each of the variables, the principal component analysis based on a variance-covariance matrix was applied to the normalized data. We made an eigenspace by using eigenvectors obtained from the principal component analysis, and all training data were projected onto the eigenspace. With this process, we can reduce the quantity of the templates, which is one of the problems of the conventional template matching method, by generating the eigenspace with the first k(<2,601) principal components. For example, if we use 50 dimensional eigenvectors, the quantity of the templates becomes 1.9 % (50/2,601) of the original data.

During testing, test data were projected onto the eigenspace described above. A test ROI was selected from the test data set and then normalized by using the mean and standard deviation of the training data set. The first k principal components of the normalized test datum were calculated with the k eigenvectors obtained by the training data set. This process projects the test ROI onto the same eigenspace as the training data set. In the next step, the CC coefficients between the test case and all the training data were calculated on the eigenspace. The maximum values of a lacunar ROI and a FP ROI were obtained. By comparing two maxima, the test ROI was distinguished. That is, if the maximum of the lacunar ROI is larger, the test ROI was distinguished as a infarct and otherwise as a FP. The CC coefficient was given as

$$\mathrm{CC}(A,B)=\frac{1}{k}\sum_{i=1}^{k}\frac{\left(A(i)-\overline{A}\right)\left(B(i)-\overline{B}\right)}{\sigma_A\sigma_B}$$

where $A(i)$ and $B(i)$ are a test datum and a training datum of ith principal components, respectively. $\overline{A}$ and $\overline{B}$ are their average values. σ_A and σ_B are the standard deviations. By performing template matching in the eigenspace, the computational complexity of the CC coefficient decreased significantly, which solves the second problem of conventional template matching.

Selection of ROI Images and Distinction Method

Because T_1- and T_2-weighted images were used in this study, there is some variation in how to select ROI images in the template matching technique. We investigated four experimental conditions.

Condition 1: 51×51 pixel ROIs were selected in a T_1-weighted image and were used for template matching in the eigenspace:

$$h_1(t)=\begin{cases}+1 & \text{if } \mathrm{CC}(T1_{\mathrm{TP}},t)-\mathrm{CC}(T1_{\mathrm{FP}},t)\geq\theta_1\\ -1 & \text{otherwise}\end{cases}$$

where $\mathrm{CC}(T1_{\mathrm{TP}},t)$ is the maximum cross-correlation value among a tth test ROI and the lacunar ROIs of the training set. CC $(T1_{\mathrm{FP}},t)$ is the maximum cross-correlation value among a tth test ROI and the FP ROIs of the training set. We compared the maximum cross-correlation value of the lacunar ROIs with that of the FP ROIs and determined the

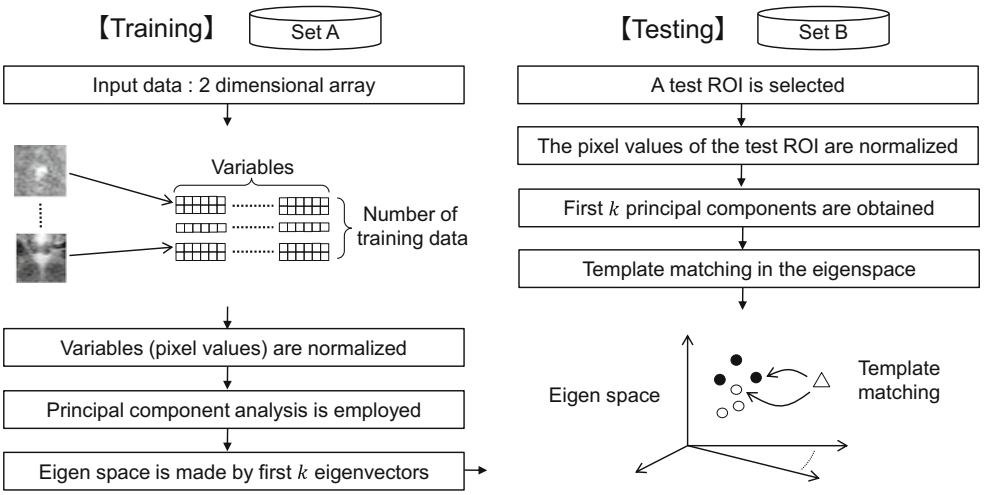

Fig. 2 Brief overview of template matching in the eigenspace (*ROI* region of interest)

test ROI to be a lacunar infarct if it was larger than threshold θ_1 and otherwise distinguished it as a FP.

Condition 2: We substituted a T_2-weighted image for the T_1-weighted image used in condition 1. The same location of the 51×51-pixel ROI was selected in the T_2-weighted image and was used for template matching in the eigenspace:

$$h_2(t) = \begin{cases} +1 & \text{if } \mathrm{CC}(T2_{\mathrm{TP}}, t) - \mathrm{CC}(T2_{\mathrm{FP}}, t) \geq \theta_2 \\ -1 & \text{otherwise} \end{cases}$$

Condition 3: We combined the result of condition 2 with that of condition 1 as follows:

$$h_3(t) = \begin{cases} +1 & \text{if } \mathrm{CC}(T1_{\mathrm{TP}}, t) - \mathrm{CC}(T1_{\mathrm{FP}}, t) \geq \theta_1 \text{ and } \mathrm{CC}(T2_{\mathrm{TP}}, t) - \mathrm{CC}(T2_{\mathrm{FP}}, t) \geq \theta_2 \\ -1 & \text{otherwise} \end{cases}$$

In condition 3, the test ROI was determined using information from both of the T_1-weighted image and the T_2-weighted image. Under conditions described above, the size of the ROI was constant. Therefore, we subsequently examined the test ROI when we unified results of different ROI sizes. For example, combinations of 31×31 and 41×41 pixel ROIs or 31×31 and 51×51 pixel ROIs were investigated.

Condition 4: In condition 3, we unified results of two different ROI sizes.

$$h_4(t) = \begin{cases} +1 & \text{if } h_3(t, \text{ROI size 1}) = 1 \text{ and } h_3(t, \text{ROI size 2}) = 1 \\ -1 & \text{otherwise} \end{cases}$$

Here, $h_3(t,\text{ROI size})$ indicates the output of condition 3 when we changed the size of the ROI. In condition 4, we distinguished between lacunar infarcts and FPs by condition 3 using two ROIs with different sizes. When the test ROI was distinguished as a lacunar infarct in both ROIs, we considered it a lacunar infarct and otherwise a FP.

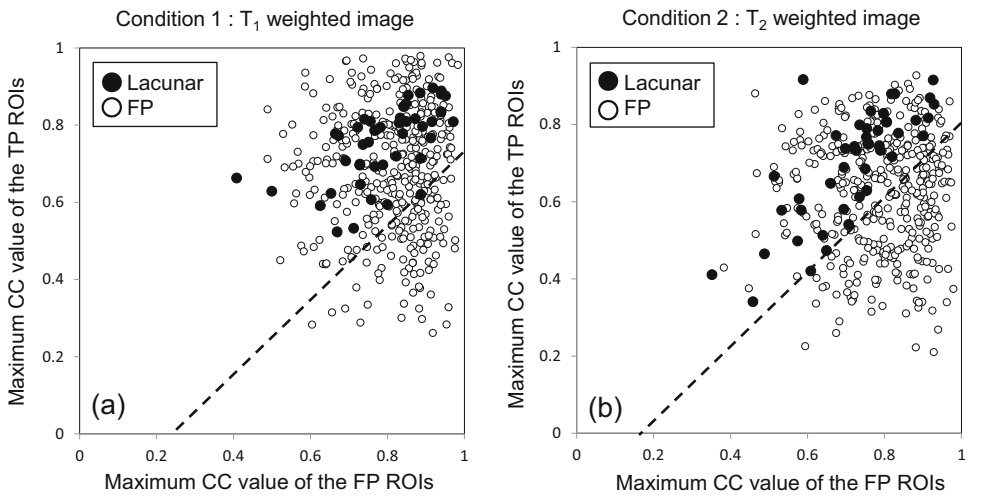

Fig. 3 Relationship between maximum cross-correlation (*CC*) value of the lacunar infarcts (*TP* true positive) ROIs and the maximum CC value of the false positive (*FP*) ROIs. *Black* and *white circles* indicate lacunar ROIs and FP ROIs, respectively. The *broken lines* were discrimination boundaries. **a** Condition 1: T_1-weighted image. **b** Condition 2: T_2-weighted image

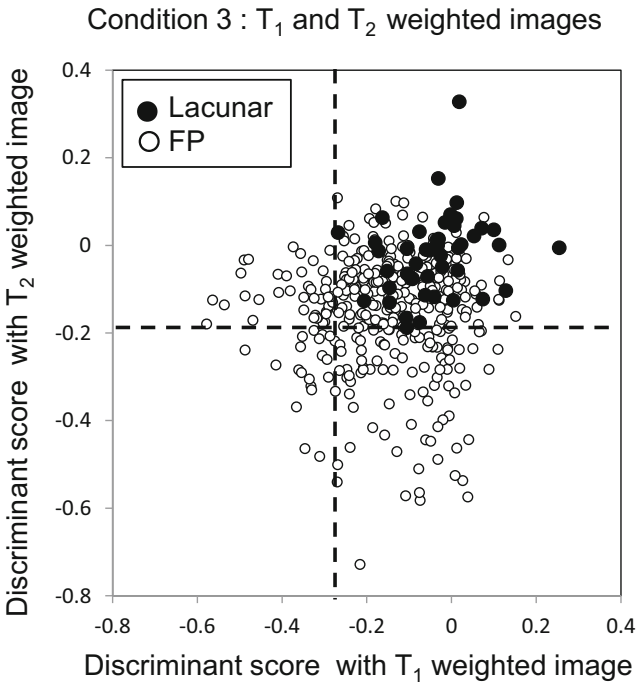

Fig. 4 .The efficacy of combining a T_1-weighted image and a T_2-weighted image. *Black* and *white circles* indicate lacunar ROIs and FP ROIs, respectively. The *broken lines* are discrimination boundaries in Fig. 2a, b. Candidates located at the upper right-hand region were classified as lacunar infarcts by the condition 3

Results

Figure 3 shows the relationship between maximum CC value of the lacunar infarcts ROIs and maximum CC value of the FP ROIs. The number of dimensions of the principal component analysis was given as 50. In the template matching, a discriminant function is given as a straight line with an inclination of 45°, because this method distinguishes test ROIs by calculating the degrees of similarity between the test ROI and both lacunar infarct ROI and FP ROI. The dashed line in Fig. 3 shows a discriminant border line when all lacunar infarcts are accurately detected. Many FPs are distributed below the discriminant border line in Fig. 3b compared with those in Fig. 3a. Therefore, we realized that T_2-weighted images had more useful information than T_1-weighted image for the distinction between lacunar infarcts and FPs.

The discriminant scores of each ROI with the T_1-weighted images are shown in Fig. 3a. Likewise, the discriminant scores of each ROI with the T_2-weighted images are also displayed in Fig. 3b. The discriminant score is given as the distance between ROI data and the discriminant boundary. Figure 4 shows the relationship between discriminant scores with a T_1-weighted image and with a T_2-weighted image. Condition 3 means that when a ROI is located at the upper right-hand region in Fig. 4, then the ROI is classified as a lacunar infarct. As shown in Fig. 4, the detection performance is improved by combining a T_1-weighted image and a T_2-weighted image.

Table 1 shows the FP reduction rates between conventional template matching and template matching in the eigenspace. The conventional template matching means template matching in the real space. We investigated the results of condition 1, condition 2, and condition 3 when the size of the ROI was changed. Template matching in the eigenspace at condition 3 with a 51×51-pixel ROI achieved the best FP reduction rate. As shown in Table 1, template matching in the eigenspace shows better performance than conventional template matching, because extra information was deleted by the principal component analysis while maintaining useful information to distinguish between lacunar infarcts and FPs.

Table 2 shows the results of condition 4 using two different ROIs. The combination of a 31×31 pixel ROI and a 51×51 pixel ROI had the best performance and was able to eliminate 34.1 % of FPs. The final performance when we added this proposed method to our previous method was

Table 1 Comparison of FP reduction rates between conventional template matching in the real space and template matching in the eigenspace. T_1, T_2, and T_1 and T_2 indicate the results of conditions 1, 2, and 3, respectively

Method		ROI size		
		31×31	41×41	51×51
Conventional template matching	T1	8.9 % (67)	6.1 % (46)	12.7 % (96)
	T2	5.4 % (41)	5.0 % (38)	14.7 % (111)
	T1 and T2	10.2 % (77)	7.8 % (59)	18.6 % (140)
Template matching in the eigenspace	T1	7.6 % (57)	5.7 % (43)	16.1 % (121)
	T2	8.6 % (65)	11.3 % (85)	24.2 % (182)
	T1 & T2	13.5 % (102)	13.8 % (104)	30.3 % (228)

The numbers in parentheses indicate the number of FP ROI that could be further eliminated in comparison of our previous scheme 8

Table 2 Results of condition 4. FP reduction rates of the combinations of three different ROI sizes

	31×31	41×41	51×51
31×31		19.0 % (143)	34.1 % (257)
41×41	–		31.2 % (235)

96.8 % (90/93) in sensitivity with 0.47 (496/1,063) FPs per slice.

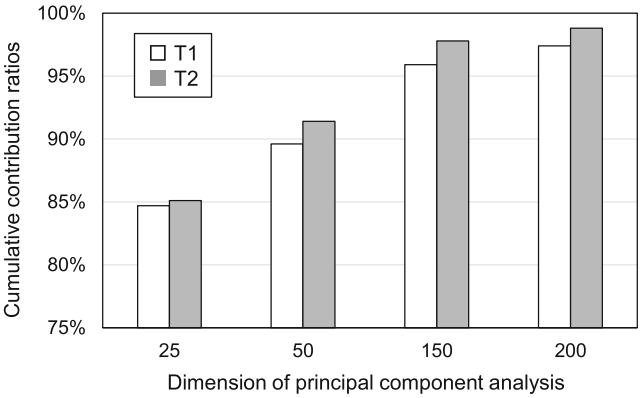

Fig. 6 Cumulative contribution ratios of the training templates by changing the dimension of principal component analysis

Discussion

We investigated the relationship between the numbers of the dimensions of the principal component analysis and FP reduction rates with a 51×51-pixel ROI. As shown in Fig. 5, the FP reduction rate was the highest when we used 50 dimensions. This tendency was the same in condition 1, condition 2, and condition 3. The quantity of the templates in 50 dimensions is 1.9 % of the original templates. However, the highest FP reduction rate was obtained. For clarifying the reason, we calculated cumulative contribution ratios of the training templates (Fig. 6). The cumulative contribution ratios of T_1-weighted images were as follows: 25 dimensions, 84.7 %; 50 dimensions, 89.6 %; 150 dimensions, 95.9 %; and 200 dimensions, 97.4 %. The cumulative contribution ratios of T_2-weighted images were as follows: 25 dimensions, 85.1 %; 50 dimensions, 91.4 %; 150 dimensions, 97.8 %; and 200 dimensions, 98.8 %. From these results, we realized that the templates in 50 dimensions retain approximately 90 % of the information of the original templates. Because the time complexity of the algorithm for calculating CC value can be expressed as $T(n)=11n+4$ where n is the size of template, the computation time becomes approximately 1/50 when we use 50 dimensional size of the template.

Figure 7 shows examples of the eliminated FPs using template matching in the eigenspace. These were classified into three types: a part of the cerebral ventricle, 54.5 %; a part of the cerebral sulcus, 38.9 %; and the enlarged Virchow-Robin spaces, 6.6 %. In our previous method, a lesion located at the center of the ROI was first extracted, and image features such as shape, size, and signal intensity were subsequently used to distinguish between lacunar infarcts and FPs [8]. Therefore, a part of the cerebral ventricle and a part of the cerebral sulcus continued to be FPs. However, because template matching takes into account image features around the lesion located at the center of the ROI, identification of these

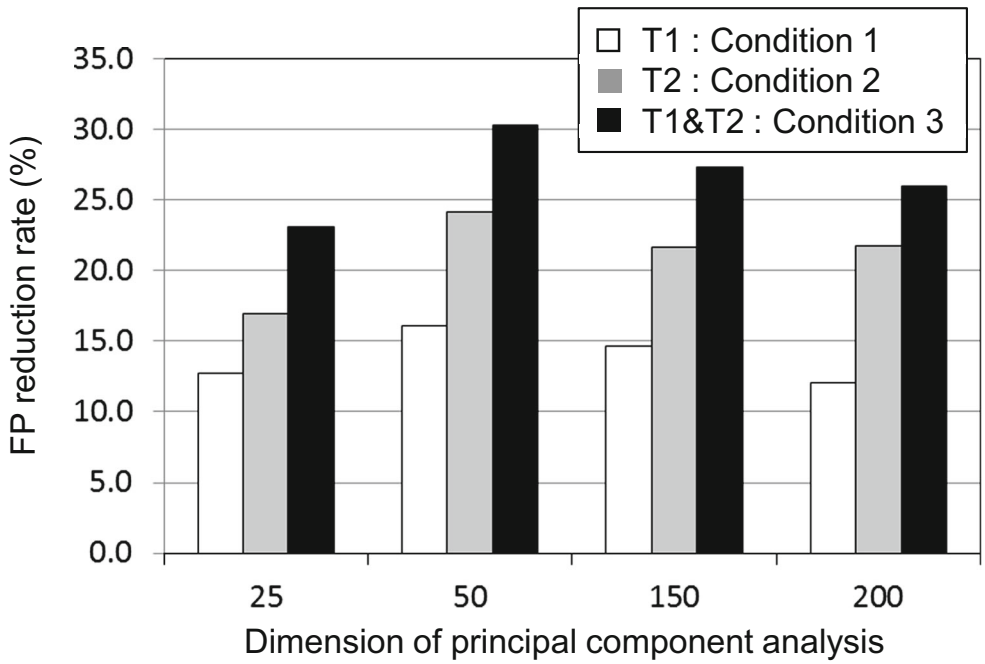

Fig. 5 FP reduction rates by changing the dimension of principal component analysis with conditions 1, 2, and 3

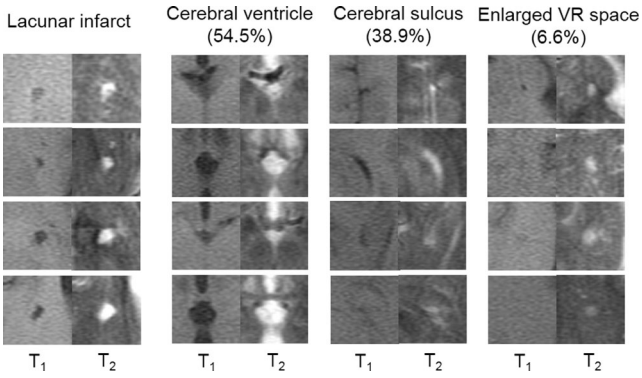

Fig. 7 Examples of eliminated false positives, which are part of the cerebral ventricle, part of the cerebral sulcus, and an enlarged Virchow-Robin (VR) space

FPs as being a part of the cerebral ventricle and the cerebral sulcus becomes easy.

Conclusion

We proposed a method using eigenspace template matching for the elimination of FPs. With this technique, the quantity of the templates became 1.9 % of conventional template matching, the computation time decreased significantly, and the number of FPs decreased from 0.71 to 0.47 per slice while maintaining a sensitivity of 96.8 %. Therefore, the modified CAD scheme could improve FP rate without a significant reduction in the true positive rate.

Acknowledgments This work was partly supported by JSPS KAKENHI Grant Number 24591815, and a Grant-in-Aid for Scientific Research on Innovative Areas 21103001 from the Ministry of Education, Culture, Sports, Science, and Technology, Japan.

References

1. Vermeer SE, Longstreth WT, Koudstaal PJ: Silent brain infarcts: a systematic review. Luncet Neurol 6:611–619, 2007
2. Kobayashi S, Okada K, Koide H, et al: Subcortical silent brain infarction as a risk factor for clinical stroke. Stroke 28:1932–1939, 1997
3. Shintani S, Shiigai T, Arinami T: Silent lacunar infarction on magnetic resonance imaging (MRI): Risk factors. J Neurol Sci 160:82–86, 1998
4. Vermeer SE, Hollander M, Dijk EJ, et al: Silent brain infarcts and white matter lesions increase stroke risk in the general population: The Rotterdam scan study. Stroke 34:1126–1129, 2003
5. Bokura H, Kobayashi S, Yamaguchi S, et al: Silent brain infarction and subcortical white matter lesions increase the risk of stroke and mortality: a prospective cohort study. J Stroke Cerebrovasc Dis 15(2): 57–63, 2006
6. Vermeer SE, Prins ND, Heijer TD, et al: Silent brain infarcts and the risk of dementia and cognitive decline. N Eng J Med 348:1215–1222, 2003
7. Yokoyama R, Zhang X, Uchiyama Y, et al: Development of an automated method for the detection of lacunar infarct regions in brain MR images. IEICE Trans Inf Syst E90-D(6):943–954, 2007
8. Uchiyama Y, Yokoyama R, Ando H, et al: Computer-aided diagnosis scheme for detection of lacunar infarcts on MR image. Acad Radiol 14(12):1554–1561, 2007
9. Uchiyama Y, Asano T, Kato H, et al: Computer-aided diagnosis for detection of lacunar infarcts on MR images - ROC analysis of radiologists' performance. J Digit Imaging 25(4):497–503, 2012
10. Lee Y, Hara T, Fujita H, et al: Automated detection of pulmonary nodules in helical CT images based on an improved template-matching technique. IEEE Trans Med Imaging 20(7):595–604, 2001
11. Li Q, Katsuragawa S, Doi K: Computer-aided diagnostic scheme for lung nodule detection in digital chest radiographs by use of a multiple-template matching technique. Med Phys 28(10):2070–2076, 2001
12. Mazurowski MA, Lo JY, Harrawood BP, et al: Mutual information-based template matching scheme for detection of breast masses: From mammography to digital breast tomosynthesis. J Biomed Inform 44(5):815–823, 2011
13. Tourassi GD, Vargas-Voracek R, Catarious DM, et al: Computer-assisted detection of mammographic masses: A template matching scheme based on mutual information. Med Phys 30(8):2123–2130, 2003
14. Kilic N, Ucan ON, Osman O: Colonic polyp detection in CT colonography with fuzzy rule based 3D template matching. J Med Syst 33(1):9–18, 2009
15. Morishita J, Katsuragawa S, Sasaki Y, et al: Potential usefulness of biological fingerprints in chest radiographs for automated patient recognition and identification. Acad Radiol 11(3):309–315, 2004
16. Murase H, Nayar SK: Illumination planning for object recognition in structured environments, Proceedings of the IEEE Conference on Computer Vision and Pattern Recognition, 31-38, June, 1994
17. Jolliffe IT: Principal component analysis, second edition, springer, 2002
18. Theodoridis S, Koutroumbas K: Pattern Recognition. Academic Press, London, 1999